A Proof of Concept of a Non-Invasive Image-Based Material Characterization Method for Enhanced Patient-Specific Computational Modeling

B. M. Fanni[1,2], E. Sauvage[3,4], S. Celi[1], W. Norman[3,4], E. Vignali[1,2], L. Landini[1,2], S. Schievano[3,4], V. Positano[1] and C. Capelli[3,4]

1. BioCardioLab, Bioengineering Unit, Fondazione Toscana Gabriele Monasterio, Via Aurelia Sud, 54100, Massa, Italy

2. Department of Information Engineering, University of Pisa, Via Girolamo Caruso 16, 56122, Pisa, Italy

3. UCL Institute of Cardiovascular Science, 20c Guilford Street, London, WC1N 1DZ, UK

4. Great Ormond Street Hospital for Children, NHS Foundation Trust, 30 Great Ormond Street, London, WC1N 3JH, UK

Corresponding author:

Simona Celi

BioCardioLab, Bioengineering Unit

Fondazione Toscana Gabriele Monasterio

Via Aurelia Sud

54100 Massa

Italy

phone: +39 0585 493644

email: s.celi@ftgm.it

Abstract

Purpose

Computational models of cardiovascular structures rely on their accurate mechanical characterization. A validated method able to infer the material properties of patient-specific large vessels is currently lacking. The aim of the present study is to present a technique starting from the flow-area (QA) method to retrieve basic material properties from magnetic resonance (MR) imaging.

Methods

The proposed method was developed and tested, first, *in silico* and then *in vitro*. *In silico*, fluid-structure interaction (FSI) simulations of flow within a deformable pipe were run with varying elastic modules (*E*) between 0.5 and 32 MPa. The proposed QA-based formulation was assessed and modified based on the FSI results to retrieve *E* values. *In vitro*, a compliant phantom connected to a mock circulatory system was tested within MR scanning. Images of the phantom were acquired and post-processed according to the modified formulation to infer *E* of the phantom. Results of *in vitro* imaging assessment were verified against standard tensile test.

Results

In silico results from FSI simulations were used to derive the correction factor to the original formulation based on the geometrical and material characteristics. *In vitro*, the modified QA-based equation estimated an average *E* = 0.51 MPa, 2% different from the *E* derived from tensile tests (i.e. *E* = 0.50 MPa).

Conclusion

This study presented promising results of an indirect and non-invasive method to establish elastic properties from solely MR images data, suggesting a potential image-based mechanical characterization of large blood vessels.

Introduction

Computational models have been widely applied over the last decades to understand the mechanics[48] and fluid dynamic[7,18] of vascular structures. With the advances of medical imaging and computational power, patient-specific, computer-based models have promised to improve substantially patients' care by personalized treatments, supporting the development of novel device and interventions.[33,45]

However, the translation of computational models into clinical applications, such as planning of procedures, is still scarce and limited to few case-reports.[5,17] Major challenges are the adaptation of computational models into patient-specific clinical conditions.[31] The use of patient-specific computational modelling, based on finite-element (FE) method, requires not only an accurate geometrical representation of the patient-specific structure, but also a translation of realistic working conditions and a faithful description of the material properties of the patient-specific case. While current imaging techniques can provide high resolution information to derive both 3D models of patient-specific anatomies and boundary conditions,[20] the *in vivo* characterization of reliable patient-specific mechanical properties still represents the biggest source of uncertainties. This lack of information causes the introduction of approximations regarding the material modelling[19,26] of patients' cardiovascular structures therefore limiting validity and applicability of computational tools. Enhanced material information, which include patient-specific information, may improve the accuracy of the numerical results, thus favoring the use of *in silico* tools in clinical practice.

Over the last years, several approaches have been explored to derive the *in vivo* patient-specific material properties of vessels in an indirect and thus non-invasive way, based on iterative FE methods and imaging data.[12,28,38,53] These strategies pointed out the importance of considering imaging information as crucial element for the mechanical inferring of vessel tissues, but the high computational cost of such techniques still limits their practical use, especially in a clinical scenario where a rapid feedback is required.

In this context, the so-called flow-area (QA) method[42,50] was shown to be a valid image-based approach to derive data related to the wall distensibility. The QA method is based on the analysis of the loop curve obtained by plotting area vs flow values during the cardiac cycle to estimate the pulse wave velocity (PWV), itself a widely accepted surrogate of arterial stiffness in clinics.[9,13,36,40,46,49] To the best of our knowledge, the QA method has not yet been tested as a potential starting point to develop a tool for the non-invasive extraction of patient-specific elastic properties (i.e. the Young's modulus) to be input in computational models.

In this study, we aimed to assess the capability of a QA-based method for inferring elastic properties of a vessel-like structure. This method was developed, first, in a controlled *in silico* environment and, then, tested within an *in vitro* MRI-compatible testbench.

Materials and Methods

In this study we first tested a standard formulation to assess its capability to derive the Young's modulus (*E*) of vessels starting from the QA method, non-invasively and requiring only imaging information. The initial formulation was tested *in silico* on a series of numerical simulations of a pulsating vessel with different *E* values assigned as input of the mechanical properties of the wall. The QA method was applied on the simulations' results to compute, first, the PWV and, then, the *E* value. The used formulation was found to be not suitable to correctly estimate the *E* values. The second step of the presented work was to derive a corrective factor in the formula. The effectiveness of the modified corrected equation was tested *in vitro* by running a MRI experiment including a deformable vessel phantom, where the inferred *E* value was verified against standard mechanical tests.

QA-Based Method to Infer the Young's Modulus

In this study the QA method was used as the starting point to derive the Young's modulus from the PWV. The QA method is an image-based tool which allow the calculation of the local PWV of a vessel based on the image assessment of flow and cross-sectional area.[50] The technique is based on the assumption that, during the reflection-free period of the cardiac cycle (i.e. the early systolic phase) the relationship between the cross-sectional area of a blood vessel and the passing flow can be approximated as a first-order linear equation. Hence, the PWV can be estimated as:

$$PWV=dQdA|||earlysystolePWV=dQdA|earlysystole \quad (1)$$

where dA is the incremental variation of the cross-sectional area and dQ is incremental variation of the flow passing through the section.

Standard Formulation

The distensibility (*D*) of a vessel wall can be defined from the inverted form of the well-known Bramwell-Hill equation[14,52]:

$$D=1\rho PWV2D=1\rho PWV2 \quad (2)$$

where ρ is the density of the fluid passing through the vessel's cross-section and the PWV can be obtained non-invasively by means of the QA method according to Eq. (1).

According to literature,[3,15,36,39] a standard estimation of the vascular wall elasticity can be further computed as:

$$ED=[3(1+A0WCSA)]DED=[3(1+A0WCSA)]D \quad (3)$$

where A_0 is the area of the lumen of the vessel and WCSA is its wall cross-sectional area (i.e. the area between the inner and the outer diameter), both measured at diastole.

The Young's modulus derived from the PWV, E_{PWV}, can be therefore defined:

$$EPWV=3\rho PWV2(1+A0WCSA)EPWV=3\rho PWV2(1+A0WCSA) \quad (4)$$

In this study, this calculation of E_{PWV} was first tested on a series of *in silico* models of a straight vessel with varying elastic modules (E_{INP}). The simulations were performed to assess the capability of the Eq. (4) to derive correctly the E value of the different implemented materials (see "In Silico Models").

Following this first campaign of computational tests, a non-linear relationship was observed between the inputted E_{INP} values and the calculated E_{PWV}.

Modified Formulation

A modification to the Eq. (4) is here presented by introducing a non-linear correction factor (κ), defined as:

$$\kappa=RAC\ \gamma\kappa=RAC\ \gamma \quad (5)$$

where the RAC is the relative area change, computed as:

$$RAC=Amax-A0AmaxRAC=Amax-A0Amax \quad (6)$$

in which A_{max} is the maximum cross-sectional area of the lumen, i.e. the area evaluated at systolic peak.

The γ parameter was derived from the simulations' results as:

$$\gamma=\sum i=1ncin\gamma=\sum i=1n cin \quad (7)$$

where c_i was based on the relationship:

$$ci=EINPRAC\ EPWVci=EINPRAC\ EPWV \quad (8)$$

for each simulation.

Hence, the modified QA-based equation to derive E (E_{OUT}) was:

$$EOUT=3RAC\ \gamma\rho PWV2(1+A0WCSA)=\kappa EPWVEOUT=3RAC\ \gamma\rho PWV2(1+A0WCSA)=\kappa EPWV \quad (9)$$

The formula introduced here aimed to take into account not only the stiffness information inferred from the PWV, retrievable from imaging, but also the area variations included in the RAC definition, opportunely adjusted by including the defined γ parameter.

In Silico Models

Numerical models were used in this study to test the initial formulation (Eq. (4)) and develop its modified version (Eq. (9)).

A two-way fluid-structure interaction (FSI) approach was adopted to simulate the flow within a model of an idealized blood vessel under pulsatile conditions. Numerical simulations were carried out with the commercial package LS-DYNA R.10 (LSTC, Livermore, USA). Fluid and solid mechanics solvers were implemented in a partitioned manner within the LS-DYNA environment and coupled using a two-way strong coupling scheme to encompass for the influence of the pulsatile fluid on the deformable structure of the vessel wall and reciprocally. The mesh deformations followed an Arbitrary Lagrangian Eulerian formulation. A tubular geometry (i.e. internal diameter of 12.7 mm and total length of 150 mm) included fluid domain and a vessel wall structure (Fig. 1a). Both domains had matching interface. A range of linear elastic isotropic materials were modelled for the vessel wall. A total of twelve simulations were carried out with different Young's moduli assigned as input (E_{INP}) of the computational model. Four cardiac cycles were simulated to allow the flow to stabilize. A time step of 0.01 s was set as a compromise between computational time and solution stability. Both fluid and solid discrete systems were considered as converged when their respective residuals dropped below threshold ε = 1.e−6 at every time step. The computational time per simulation depended on the value of Young's modulus with smaller moduli yielding longer simulations.

Figure 1

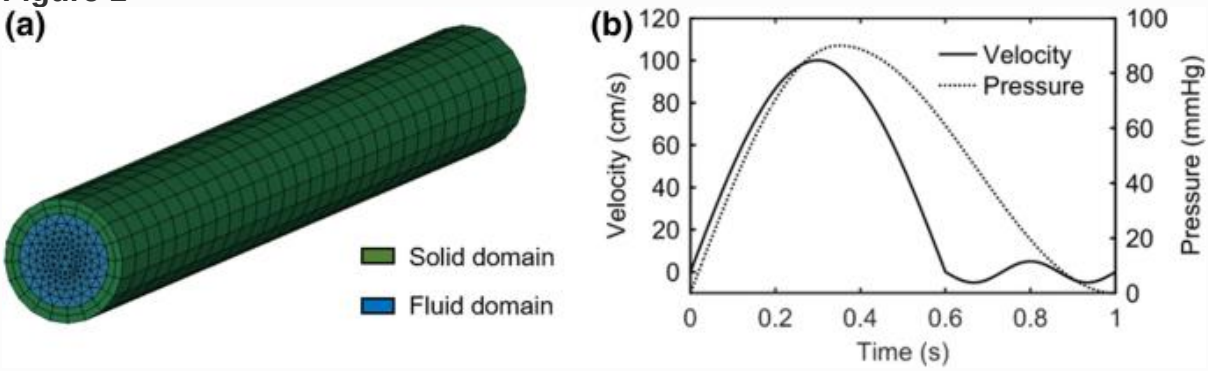

(a) Mesh of the vessel model, including solid (green elements) and fluid (blue elements) domains; (b) Velocity and pressure profiles assigned as inflow and outflow boundary conditions, respectively.

Fluid Domain

The unsteady fluid computation analysis was performed using the incompressible flow solver ICFD implemented in LS-DYNA. The geometry was meshed with 18,166 tetrahedral elements in the open source software Gmsh (http://gmsh.info/).[30] Preliminary mesh convergence study was performed to confirm a mesh-independent solution. Fluid simulated was water, thus modelled as an incompressible and Newtonian fluid with a density of 998 kg m^{-3} and a dynamic viscosity of 0.001 kg m^{-1} s^{-1}. Periodic boundary conditions were set up to impose velocity at the inlet and pressure at the outlet (Fig. 1b).

The fluid behavior is governed by the Navier–Stokes equations. The ICFD solver discretizes the governing equations using a low-order continuous finite element method.

Structural Domain

The structural model consisted in a hollow cylinder surrounding the fluid domain. Thickness of the wall was 2 mm. Following mesh sensitivity analysis, the geometry was meshed in Gmsh environment with 1200 hexahedral elements. A linear elastic material was implemented. A total of twelve simulations were run with E_{INP} values varying from 0.50 to 32 MPa, with an oversampling in the region close to 1 MPa. A Poisson ratio of 0.47, typical of elastomeric materials, was set. The structural model was constrained with fixed ends.

The governing equations for the solid part are those of the of linear elasticity (small deformations). Similarly to fluid domain, LS-DYNA discretizes the equations of linear elasticity with continuous finite element method.

Simulations Post-processing

The results of the FSI simulations were post-processed and then used to test, initially, the starting Eq. (4) to estimate the *E* value and then, following that it was not suitable for a correct inferring, to refine the formula with the inclusion of the correction factor (Eq. (9)). The post-processing was performed on the last cycle simulated. Flow and area data were extracted in the middle cross-section of the FSI models. Cross-sectional area and through-plane flow values were analyzed over time with the open source tool ParaView (https://www.paraview.org/).1

In Vitro Experiment

The proposed QA-based equations were also applied *in vitro* using an image acquisition protocol routinely used in clinics. The aim of the experiment was twofold: to confirm that Eq. (4) was not a suitable tool to infer the correct Young's modulus from imaging and to verify that the corrected formula as previously defined *in silico* (Eq. (9)) provided better outcomes.

A deformable cylindrical phantom was inserted within a mock circulation loop reproducing pulsatile flow conditions. MR images were acquired and processed to retrieve both area and flow values. These data were used to retrieve the Young's modulus of the material phantom according respectively to Eq. (4) (E_{PWV}) and Eq. (9) (E_{MRI}). The results were compared to the Young's modulus directly derived from standard tensile tests (E_{TT}). Details of the experiment are reported in the next paragraphs.

Phantom

The deformable phantom was manufactured with TangoPlus material, 3D printed with an Objet500 Connex 3D printer (Stratasys, Minnesota, USA). The material was chosen as commonly used to mimic great vessels.[6,10] The geometry of the phantom replicated the numerical model (i.e. internal diameter = 12.7 mm, thickness = 2 mm and length = 150 mm).

Tensile Tests

The 3D printed TangoPlus material was mechanically evaluated with standard uniaxial tensile tests by using a custom-made and fully-controlled extensometer system already used by our group.[29] The specimens were 3D printed in three different orientations (with fibers aligned along horizontal, vertical and oblique directions, respectively), in order to assess the effect of the printing direction on the mechanical properties of the material. Five samples were fabricated for each group, for a total of fifteen specimens. The directives of the regulation for elastomeric materials (ASTM D 412 06a) were followed for the design and the testing of the specimens to derive the Young's modulus of the 3D printed TangoPlus material (E_{TT}).

Mock Circulatory Loop

The TangoPlus phantom was inserted within an experimental set-up consisting of a mock circulatory loop equipped with flow and pressure sensors as depicted in Fig. 2. The mock loop replicated cardiac-like pulsatile conditions by means of a two-element Windkessel model. The pulsatile pump was the Harvard apparatus (Massachusetts, USA) with capability to set stroke volume (SV), heart rate (HR) and diastolic time fraction (DTF). Sensors were positioned to monitor continuously flow and pressure signals in proximity of the phantom during the pulsatile conditions imposed by the pump. A Transonic 9PXL perivascular ultrasound clamp-on probe (Transonic Systems, New York, USA) was used as flow sensor. A fiber optic pressure wire (Opsens, Quebec, Canada) was used as pressure sensor. The compliance of the system was represented by the compliant phantom itself. Resistance was implemented by using a metered needle-pinch valve. All the components were connected by flexible but not compliant Tygon pipes.

Figure 2

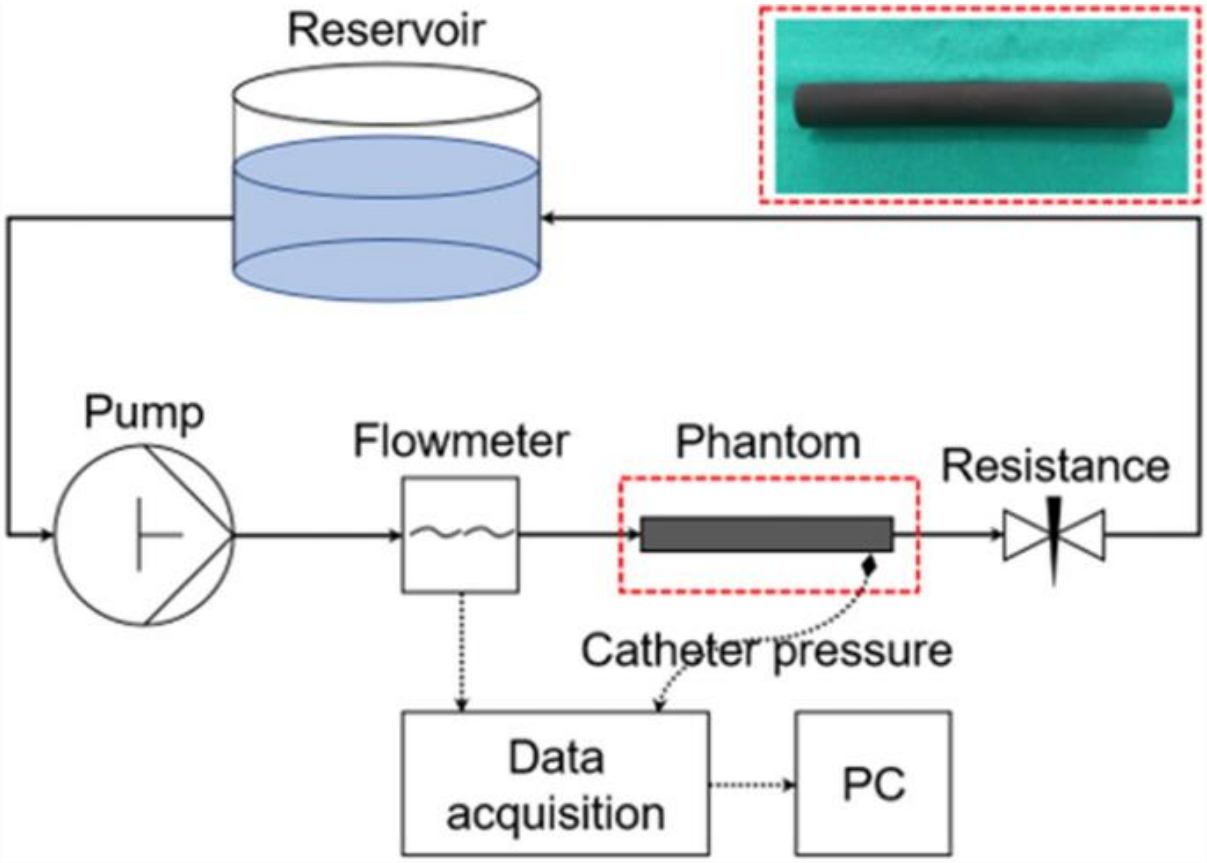

Representative scheme of the mock loop circuit, including the pulsatile pump, the flow and pressure sensors, the data acquisition system, the phantom, the resistance and the reservoir.

PC MRI Acquisition and Processing

The MRI scanner used for the acquisition was Siemens Avanto 1.5 T (Siemens Healthcare, Erlangen, Germany), available at our clinical centre. Balanced steady-state free precession PC MRI was the selected imaging technique to measure flow and area variations of the phantom subjected to the pulsatile conditions. The MRI acquisitions were performed in two experimental conditions (hereafter called *Condition 1* and *Condition 2*) with varying pump settings in terms of SV, HR and DTF (Table 1). Each MRI acquisition resulted in 40 PC MRI frames, acquired at the middle cross-section of the phantom. Standard acquisition parameters set for clinical acquisitions were used for both experimental conditions (Table 2).

Table 1 List of the pump settings used for the two MRI acquisitions.

Setting	**Value**	
	Condition 1	***Condition 2***
SV	40 (mL)	50 (mL)
HR	60 (bpm)	70 (bpm)

Setting	Value	
	Condition 1	***Condition 2***
DTF	50/50	45/55

Table 2 List of the acquisition parameters used for the two MRI acquisitions.

Acquisition parameter	Value	
	Condition 1	***Condition 2***
Acquisition matrix	192 × 256	240 × 320
Frames	40	40
Time increment	23.525 (ms)	19.725 (ms)
Flip angle	30 (degrees)	30 (degrees)
Echo time	2.18 (ms)	2.33 (ms)
Repetition time	29.9 (ms)	30.75 (ms)
Pixel size	1.17 × 1.17 (mm^2)	0.94 × 0.94 (mm^2)
Slice thickness	5 (mm)	5 (mm)
VENC	200 ($cm\ s^{-1}$)	200 ($cm\ s^{-1}$)

After the acquisition, PC MRI data of the phantom were processed to estimate the elastic module of TangoPlus based on imaging information according to both Eqs. (4) and (9).

Analysis of the PC images were performed using the software Segment v2.0 (http://segment.heiberg.se),4 whose vessel tracking algorithm allowed to identify the phantom contours. A user-defined region of interest was drawn to define the vessel boundary in each frame from which the phantom cross-sectional area and through plane flow throughout the cardiac cycle were obtained.

Results

In Silico Data Results

All the FSI simulations were stable and reached solution convergence. For all the E_{INP} values used in the simulations (Fig. 3a), the corresponding QA loops were computed (Fig. 3b) as based on the flow (Fig. 3c) and area (Fig. 3d) information extracted from the middle cross-section of the computational models. Figs. 3c and 3d confirm how the averaged through-plane flow in the middle cross-section during the cardiac cycle is equivalent for all simulations and how the area deformation strongly depended on the E_{INP} value of the material. In particular, area variations decreased consistently with increasing stiffness. All the obtained QA loops (Fig. 3b) were linearly interpolated in correspondence of the early systole period. Linear fitting resulted in a R^2 value of 0.99 ± 0.008 (n = 12). The analysis of the QA loops (Fig. 3b) led to the values as listed in Table 3.

Figure 3

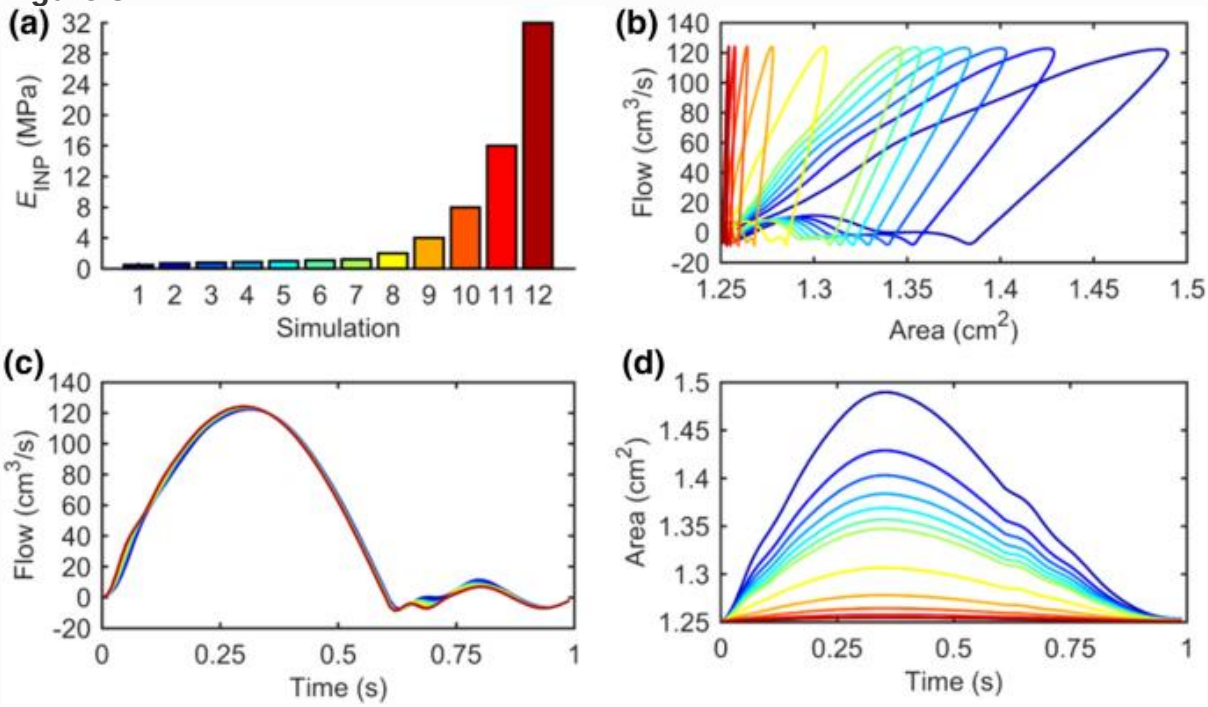

(a) Values of the Young's moduli assigned as input for the simulations, ranging from the softer 0.5 MPa (dark blue) to the stiffer 32 MPa (dark red); (b) QA loop curves as obtained from the FSI datasets analysis; (c) Area values along the cardiac cycle as extracted from the FSI datasets analysis; (d) Flow values along the cardiac cycle as extracted from the FSI datasets analysis.

Table 3 List of the resulted PWV, E_{PWV}, RAC, κ and E_{OUT} values related to the E_{INP} values assigned in the simulations.

Simulation	E_{INP} (MPa)	PWV (m s^{-1})	E_{PWV} (MPa)	RAC	κ	E_{OUT} (MPa)
1	0.5	5.86	0.24	0.159	2.016	0.49
2	0.7	7.74	0.42	0.123	1.565	0.66
3	0.8	8.95	0.57	0.107	1.363	0.77
4	0.9	9.63	0.66	0.095	1.207	0.79
5	1.0	10.91	0.84	0.085	1.083	0.91
6	1.1	12.18	1.05	0.077	0.982	1.03
7	1.2	13.45	1.28	0.071	0.898	1.15
8	2	23.45	3.89	0.042	0.534	2.08
9	4	48.17	16.41	0.021	0.266	4.36
10	8	97.67	67.46	0.010	0.132	8.93
11	16	196.62	273.38	0.005	0.066	18.07
12	32	394.75	1101.92	0.003	0.033	36.36

The γ parameter (Eq. (7)) resulted to be 12.69 ± 1.12 (n = 12). Its mean value (γ = 12.69) was used to compute the κ factor, together with the RAC parameter, according to Eq. (5).

Table 3 reports the resulting E_{PWV} and E_{OUT} derived respectively from the basic formulation (Eq. (4)) and its proposed modification (Eq. (9)), together with the PWV, RAC and κ parameters.

In Vitro Data Results

The segmentation throughout the cardiac cycle of the two acquired PC MRI datasets resulted in the curves as shown in Fig. 4a for *Condition 1* and Fig. 4b for *Condition 2*. QA loops are depicted in Figs. 4c and 4d for *Condition 1* and *Condition 2*, respectively. Following interpolation of the data during early systole (R^2 = 0.99 ± 0.001, n = 2), the calculated PWV, E_{PWV}, RAC, κ and E_{MRI} values are reported in Table 4. The E_{MRI} value of the TangoPlus material as extracted from the proposed modified equation (Eq. (9)) resulted to be 0.51 ± 0.04 MPa (n = 2). For the calculation of the E_{MRI} values (Eq. (9)), the γ parameter was maintained as calculated from *in silico* analyses (γ = 12.69).

Figure 4

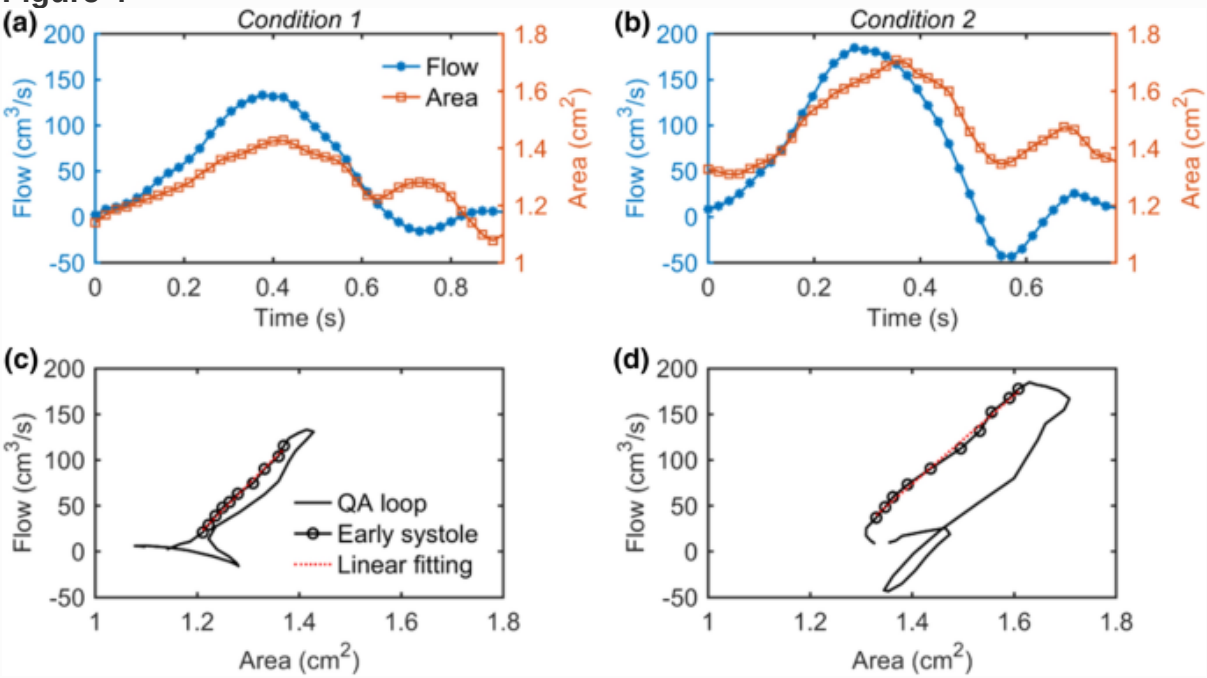

In the top panels, time-dependent through-plane flow (blue line with star markers) and cross-sectional area (orange line with square markers) curves, as extracted from the PC MRI datasets segmentation for Condition 1 (a) and Condition 2 (b). In the bottom panels, QA loops (black line) with highlighted points of the early systole period (black circle markers) and linear fitting (dotted red line) for Condition 1 (c) and Condition 2 (d).

Table 4 List of the resulted PWV, E_{PWV}, RAC, κ and E_{MRI} values for the two experimental conditions.

Condition	**PWV (m s^{-1})**	**E_{PWV} (MPa)**	**RAC**	**κ**	**E_{MRI} (MPa)**
1	5.57	0.21	0.202	2.560	0.54
2	4.84	0.17	0.223	2.830	0.48

The results of E_{MRI} values were found to be in accordance with the E_{TT} value as derived from the tensile tests of TangoPlus, with a percentage error of 2%.

The printing direction resulted to not affect the mechanical properties of the TangoPlus, thus confirming an isotropic behavior. For each sample printed with the three different fibers orientations, the resulted average stress–strain curve and the corresponding linear fitting curve are shown in Fig. 5. The resulting E_{TT} value was 0.50 ± 0.02 MPa with a R^2 value of 0.99 ± 0.001 (n = 15).

Figure 5

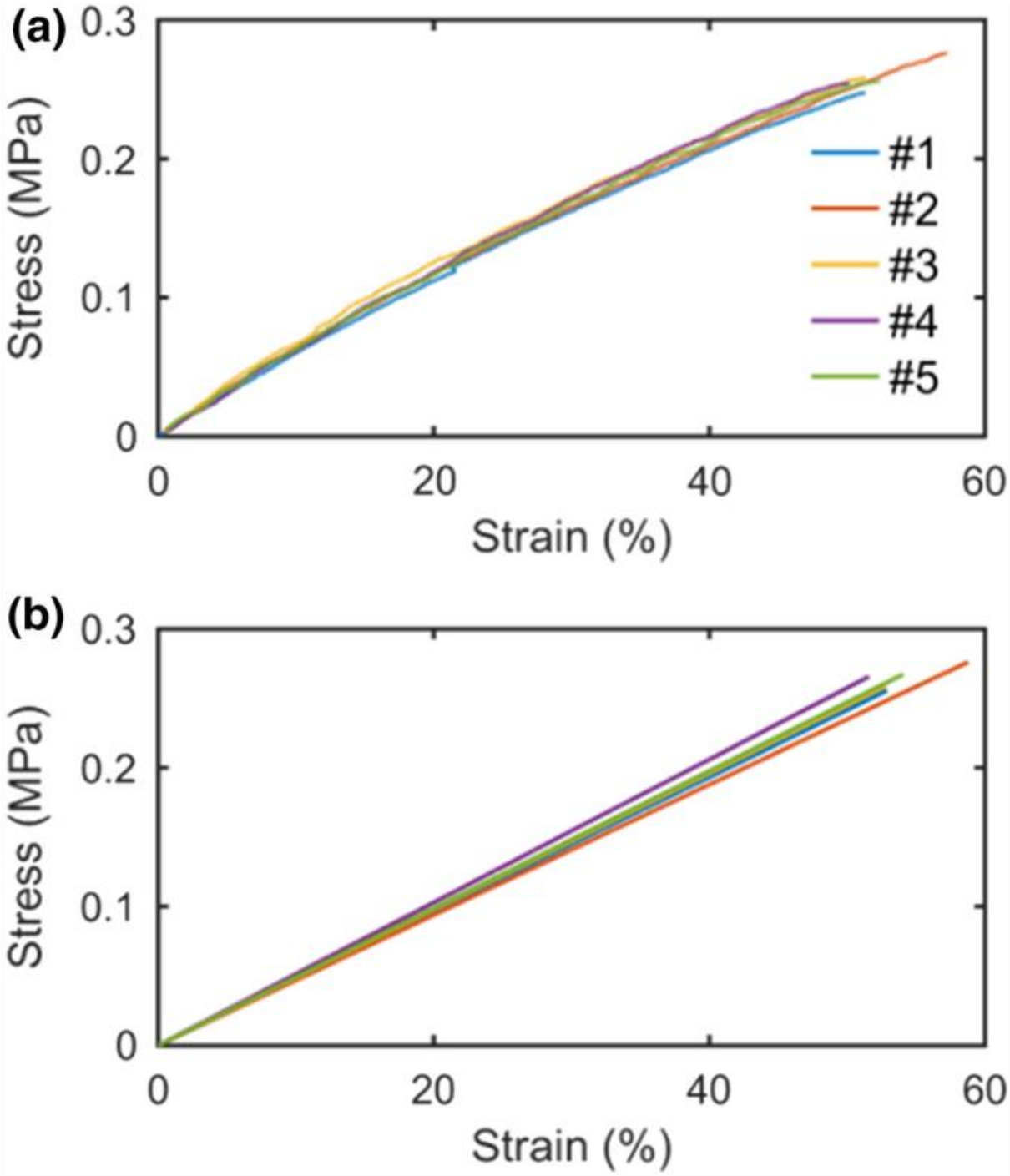

Average stress–strain curves resulted from tensile tests (a) and related linear interpolation curves (b).

Discussion and Conclusions

In this work, a non-invasive, indirect approach based on the QA method for the assessment of basic mechanical properties of vessel's models was investigated. The findings of our study propose a modified formulation based on the QA method to be used to derive a surrogate of the elastic module, suitable to be used in numerical simulations.

The QA method used in this study was developed first by Vulliémoz et al.[50] to estimate the stiffness of specific vascular structures as based on MRI and then by Rabben at al.[42] by using ultrasound images. The QA method has become a widely used tool to assess the arterial stiffness in terms of PWV in an indirect way.[32,41,51] Recent studies have also explored the potentiality of the MRI technique, demonstrating the capability of 4D Flow MRI to provide PWV assessments[43] and information related to the material properties if coupled with pressure data.[24,54] The present study explored a method to extract material parameters (i.e. Young's modulus) directly from 2D image analysis with no need of invasive pressure measurements. This approach using a different formulation[2,22] and consistent with the one used in this work,[39] was already suggested in the literature, but to the best of our knowledge not assessed with a campaign of *in silico* and *in vitro* tests.

In silico, a computational campaign allowed us to test, amend and enhance the initial proposed formulation (Eq. (4)). In particular, this allowed us to refine the accuracy of the predictions of the proposed QA-based method on a wide range of linear elastic materials with E ranging from 0.50 to 32 MPa. The values were chosen to optimize the methodology especially around the physiological range of Young's moduli used in numerical models for cardiovascular structures.[7,11,16,54] The numerical campaign showed how the original formulation (Eq. (4)) did indeed provide an overall good indicator of the wall stiffness but was not suitable to infer the correct Young's modulus, as demonstrated by the huge non-linearity between input and inferred values (Figs. 6a and 6b). Importantly, this allowed us to quantify a correction factor for Eq. (4).

Figure 6

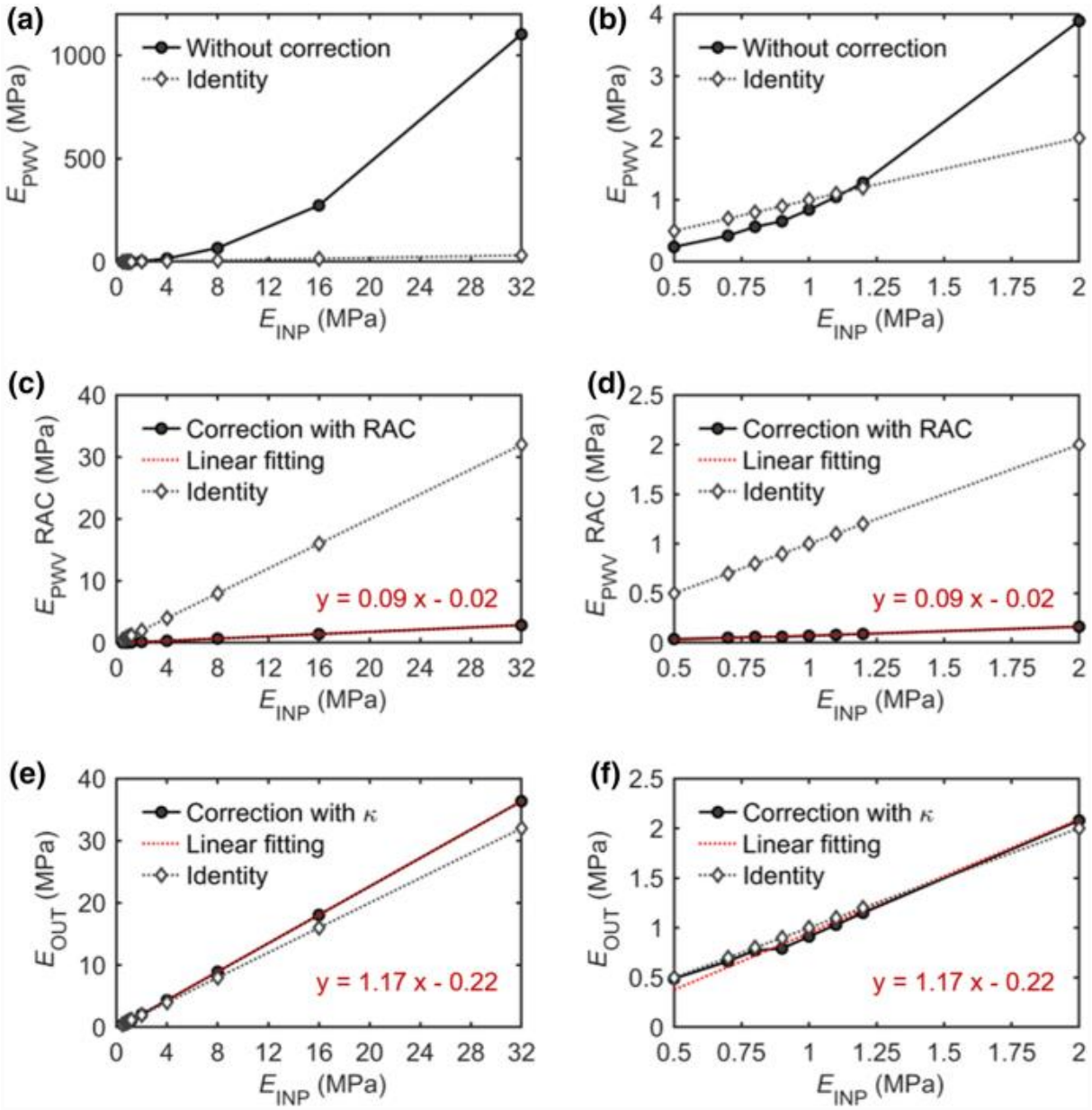

(a) Non-linear trend of the inferred E_{PWV} values as derived from Eq. (4) in respect to the E_{INP} values (black line with circle markers); (b) Magnified view of panel (a) in the range 0.5–2 MPa; (c) Trend of the inferred values after correction with solely the RAC parameter in respect to the E_{INP} values (black line with circle markers) and linear interpolation overlapped (dotted red line) with fitting equation; (d) Magnified view of panel (c) in the range 0.5–2 MPa; (e) Trend of the inferred E_{OUT} values as obtained from Eq. (9) after correction with the κ factor in respect to the E_{INP} values (black line with circle markers) and linear interpolation overlapped (dotted red line) with fitting equation; (f) Magnified view of panel (e) in the range 0.5–2 MPa.

In particular, the addition of the RAC parameter, which is used in clinics for the assessment of vessels' state,[34,44,47] encompasses for overall cross-sectional area changes during the cardiac cycle, namely maximum and minimum areas (Eq. (6)), resulting in a clear reduction of the non-linearity initially encountered but not yet sufficient to accomplish for the overlapping between $E_{INP} - E_{OUT}$ curve and the identity line (Figs. 6c and 6d). The complete correction factor, namely κ (Eq. (5)),

also includes the parameter γ (Eq. (7)) which was derived empirically from the analysis of all the simulations' results. The proposed modified equation (Eq. (9)) resulted in a linear correspondence between E_{OUT} and E_{INP} (Figs. 6e and 6f). The γ factor was defined in this study as the average of the c_i values computed for each of the twelve run simulations (Eq. (8)). As result γ was 12.69 ± 1.12 (n = 12). The low standard deviation of γ, lower than 10%, was a positive outcome as may demonstrate its independence on the E value of the material, opening up that further investigations may lead to its full parametrization.

However, it is worth to note that the strategy adopted here is based on the a priori knowledge of the E_{INP} values for the definition of γ. For this reason, the method was blindly tested on an *in vitro* experiment and it was found to derive accurately the elastic modulus.

In particular, this experiment confirmed excellent agreement between the E_{MRI} value (0.51 ± 0.04 MPa) and the E_{TT} value (0.5 ± 0.02 MPa). The error between E_{MRI} (Eq. (9)) and E_{TT} was only 2.0% compared to the 62% difference between E_{PWV} (Eq. (4)) and E_{TT}. The results of the experiment showed that the standard formulation (Eq. (4)) is probably not suitable to infer the real E value of the material and that the inclusion of a corrective factor is necessary for a correct prediction. Moreover, the experimental approach allowed to use real imaging data as starting point of the workflow, from the application of the QA method to the estimation of the Young's modulus of the phantom.

A further refinement of the methodology here presented can potentially lead to a novel technique to quantify the *in vivo* local mechanical characteristics of great vessels in a non-invasive way. This could likely contribute to reduce the uncertainty of patient-specific simulations and therefore to facilitate their translation to clinics. This might enhance simulations of device implantation, as in the case of pulmonary[8] or aortic valve[23] replacement, where a realistic implementation of the structural response of the patient-specific vessel wall tissue is critical to predict the correct intervention outcome. The proposed workflow followed in this investigation is promising per itself is promising as it moves from only *in silico* results to correct a theoretical methodology. As a proof of concept, the predictive capability of the presented modified formula (Eq. (9)) was confirmed on *in vitro* tests which are less controllable and then closer to *in vivo* case.

Limitations

Although the preliminary results here presented are promising, future works are necessary to overcome the current limitations of the presented study and to investigate more relevant physiological conditions. First, the modelled cylinder has a size which is comparable to the big vessel, but it cannot represent the complexity of a realistic vessel shape characterized by bending regions and irregularities. This choice comes from the will to assess the presented methodology on a simple setting before moving on more challenging scenarios. Thus, more realistic vessel shapes, including idealized anatomies and patient-specific geometries will be tested to further refine the proposed QA-based technique, both *in silico* and *in vitro*. In the same way, boundary conditions will need further assessment. In fact, both inlet, i.e. prescribed

velocity, and outlet, i.e. prescribed pressure, boundary conditions were simplified in the initial *in silico* campaign in view of the *in vitro* replica to be as close as possible to the numerical simulations settings (Fig. 1b). In particular, the velocity profile was built in accordance to the capabilities of the Harvard apparatus pump to provide selected waveforms. The implemented pressure range (0–90 mmHg) was prescribed to maintain the analysis at a generic level, taking into account for a full range of pre-loaded configurations. Future studies will explore both population average and patient-specific conditions. The simulated fluid was water and no blood-equivalent solutions were used. Albeit this choice was in line with previous in vitro cardiovascular studies,[21,25,27,35,37] the effect of blood properties will be included in the next steps to explore the effect due to different values of density and viscosity. Finally, the proposed formulation will be tested to other compliant materials, including anisotropic and non-homogenous materials and considering viscoelastic and hyperelastic behaviours.

These future works would enhance the confidence of the predictive results provided by the proposed method, thus facilitating the translation of its applicability on *in vivo* patients' imaging data for a retrospective analysis.

To conclude, the present study lays strong basis for the use of an indirect and non-invasive technique, to derive elastic properties of vessel-like models from solely bi-dimensional PC MRI data, which is routinely acquired in patients referred for cardiovascular interventions.

References

1. Ahrens, J., B. Geveci, and C. Law. ParaView : an end-user tool for large data visualization. Energy 836:717–732, 2005.

2. Avril, S., J. M. Huntley, and R. Cusack. In vivo measurements of blood viscosity and wall stiffness in the carotid using PC-MRI. Eur. J. Comput. Mech. 18(1):9–20, 2009.
MATH

3. Bézie, Y., J. M. Lamazière, S. Laurent, P. Challande, R. S. Cunha, J. Bonnet, et al. Fibronectin expression and aortic wall elastic modulus in spontaneously hypertensive rats. Arterioscler. Thromb. Vasc. Biol. 18(7):1027–1034, 1998.

4. Bidhult, S. L., M. Carlsson, K. Steding-Ehrenborg, H. Arheden, and E. Heiberg. A new method for vessel segmentation based on a priori input from medical expertise in cine phase-contrast magnetic resonance imaging. J. Cardiovasc. Magn. Reson. 16(1):P355, 2014.

5. Biglino, G., C. Capelli, J. Bruse, G. M. Bosi, A. M. Taylor, and S. Schievano. Computational modelling for congenital heart disease: how far are we from clinical translation? Heart 103(2):98–103, 2017.

6. Biglino, G., P. Verschueren, R. Zegels, A. M. Taylor, and S. Schievano. Rapid prototyping compliant arterial phantoms for in-vitro studies and device testing. J. Cardiovasc. Magn. Reson. 15(1):2, 2013.

7. Boccadifuoco, A., A. Mariotti, S. Celi, N. Martini, and M. V. Salvetti. Impact of uncertainties in outflow boundary conditions on the predictions of hemodynamic simulations of ascending thoracic aortic aneurysms. Comput. Fluids 30(165):96–115, 2018.
MathSciNet MATH

8. Bonhoeffer, P., Y. Boudjemline, Z. Saliba, J. Merckx, Y. Aggoun, D. Bonnet, et al. Percutaneous replacement of pulmonary valve in a right-ventricle to pulmonary-artery prosthetic conduit with valve dysfunction. Lancet 356(9239):1403–1405, 2000.

9. Boonyasirinant, T., P. Rajiah, and S. D. Flamm. Abnormal aortic stiffness in patients with bicuspid aortic valve: phenotypic variation determined by magnetic resonance imaging. Int. J. Cardiovasc. Imaging 35(1):133–141, 2019.

10. Bosi, G. M., B. Biffi, G. Biglino, V. Lintas, R. Jones, S. Tzamtzis, et al. Can finite element models of ballooning procedures yield mechanical response of the cardiovascular site to overexpansion? J Biomech. 49(13):2778–2784, 2016.

11. Bosi, G. M., C. Capelli, M. H. Cheang, N. Delahunty, M. Mullen, A. M. Taylor, et al. Population-specific material properties of the implantation site for transcatheter aortic valve replacement finite element simulations. J. Biomech. 11(71):236–244, 2018.

12. Bosi, G. M., C. Capelli, S. Khambadkone, A. M. Taylor, and S. Schievano. Patient-specific finite element models to support clinical decisions: a lesson learnt from a case study of percutaneous pulmonary valve implantation. Catheter. Cardiovasc. Interv. 86(6):1120–1130, 2015.

13. Boutouyrie, P., A. I. Tropeano, R. Asmar, I. Gautier, A. Benetos, P. Lacolley, et al. Aortic stiffness is an independent predictor of primary coronary events in hypertensive patients: a longitudinal study. Hypertension 39(1):10–15, 2002.

14. Bramwell, J. C., and A. V. Hill. The velocity of pulse wave in man. Proc. R. Soc. Lond. B 93(652):298–306, 1922.

15. Bussy, C., P. Boutouyrie, P. Lacolley, P. Challande, and S. Laurent. Intrinsic stiffness of the carotid arterial wall material in essential hypertensives. Hypertension 35(5):1049–1054, 2000.

16. Campobasso, R., F. Condemi, M. Viallon, P. Croisille, S. Campisi, and S. Avril. Evaluation of peak wall stress in an ascending thoracic aortic aneurysm using FSI simulations: effects of aortic stiffness and peripheral resistance. Cardiovasc. Eng. Technol. 9(4):707–722, 2018.

17. Capelli, C., E. Sauvage, G. Giusti, G. M. Bosi, H. Ntsinjana, M. Carminati, et al. Patient-specific simulations for planning treatment in congenital heart disease. Interface Focus 8(1):20170021, 2018.

18. Capellini, K., E. Vignali, C. Emiliano, E. Gasparotti, M. E. Biancollini, L. Landini, et al. Computational fluid dynamic study for aTAA hemodynamics: an integrated image-based and radial basis functions mesh morphing approach. J. Biomech. Eng., 140(11):111007, 2018.

19. Celi, S., S. Berti. Biomechanics and FE modelling of aneurysm: review and advances in computational models. In: Y. Murai (ed.) Aneurysm, Chap. 1. InTech, 2012.

20. Celi, S., N. Martini, L. E. Pastormerlo, V. Positano, and S. Berti. Multimodality imaging for interventional cardiology. Curr. Pharm. Des. 23(22):3285–3300, 2017.

21. Choi, J.-W., J. H. Choe, S. Y. Jung, H. Park, and H. Ha. Fabrication of affordable pulse duplication system for the in-vitro cardiovascular experiments based on gear pump and orifice flowmeter. J. Mech. Sci. Technol. 33(8):3927–3932, 2019.

22. Coolen, B. F., C. Calcagno, P. van Ooij, Z. A. Fayad, G. J. Strijkers, and A. J. Nederveen. Vessel wall characterization using quantitative MRI: what's in a number? MAGMA 31(1):201–222, 2018.

23. Cribier, A., H. Eltchaninoff, A. Bash, N. Borenstein, C. Tron, F. Bauer, et al. Percutaneous transcatheter implantation of an aortic valve prosthesis for calcific aortic stenosis. Circulation 106(24):3006–3008, 2002.

24. D’Souza, G. A., M. D. Taylor, and R. K. Banerjee. Evaluation of pulmonary artery wall properties in congenital heart disease patients using cardiac magnetic resonance. Prog. Pediatr. Cardiol. 1(47):49–57, 2017.

25. de Beaufort, H. W. L., M. Coda, M. Conti, T. M. J. van Bakel, F. J. H. Nauta, E. Lanzarone, et al. Changes in aortic pulse wave velocity of four thoracic aortic stent grafts in an ex vivo porcine model. PLoS ONE 12(10):e0186080, 2017.

26. Di Achille, P., S. Celi, F. Di Puccio, and P. Forte. Anisotropic AAA: computational comparison between four and two fiber family material models. J. Biomech. 44(13):2418–2426, 2011.

27. Di Puccio, F., S. Celi, and P. Forte. Review of experimental investigations on compressibility of arteries and introduction of a new apparatus. Exp. Mech. 52(7):895–902, 2012.

28. Flamini, V., A. P. Creane, C. M. Kerskens, and C. Lally. Imaging and finite element analysis: a methodology for non-invasive characterization of aortic tissue. Med. Eng. Phys. 37(1):48–54, 2015.

29. Gasparotti, E., E. Vignali, P. Losi, M. Scatto, B. M. Fanni, G. Soldani, et al. A 3D printed melt-compounded antibiotic loaded thermoplastic polyurethane heart valve ring design: an integrated framework of experimental material tests and numerical simulations. Int. J. Polym. Mater. Polym. Biomater. 68(1–3):1–10, 2019.

30. Geuzaine, C., and J.-F. Remacle. Gmsh: a 3-D finite element mesh generator with built-in pre- and post-processing facilities. Int. J. Numer. Methods Eng. 79(11):1309–1331, 2009.
MathSciNet MATH

31. Huberts, W., S. G. H. Heinen, N. Zonnebeld, D. A. F. van den Heuvel, J.-P. P. M. de Vries, J. H. M. Tordoir, et al. What is needed to make cardiovascular models suitable for clinical decision support? A viewpoint paper. J. Comput. Sci. 24:68–84, 2018.

32. Ibrahim, E. Accurate method for measuring arterial pulse wave velocity by cardiovascular magnetic resonance. J. Cardiovasc. Magn. Resonan. 14(Suppl 1):O12, 2012.

33. Keshavarz-Motamed, Z., J. Garcia, and L. Kadem. Mathematical, numerical and experimental study in the human aorta with coexisting models of bicuspid aortic stenosis and coarctation of the aorta. Conf. Proc. IEEE Eng. Med. Biol. Soc. 2011:182–185, 2011.

34. Kheyfets, V. O., M. Schafer, C. A. Podgorski, J. D. Schroeder, J. Browning, J. Hertzberg, et al. 4D magnetic resonance flow imaging for estimating pulmonary vascular resistance in pulmonary hypertension. J. Magn. Reson. Imaging 44(4):914–922, 2016.

35. Knoops, P. G., G. Biglino, A. D. Hughes, K. H. Parker, L. Xu, S. Schievano, et al. A mock circulatory system incorporating a compliant 3D-printed anatomical model to investigate pulmonary hemodynamics. Artif. Organs 41(7):637–646, 2017.

36. Laurent, S., J. Cockcroft, L. Van Bortel, P. Boutouyrie, C. Giannattasio, D. Hayoz, et al. Expert consensus document on arterial stiffness: methodological issues and clinical applications. Eur. Heart J. 27(21):2588–2605, 2006.

37. Liu, Y., P. Allaire, H. Wood, and D. Olsen. Design and initial testing of a mock human circulatory loop for left ventricular assist device performance testing. Artif. Organs 29(4):341–345, 2005.

38. Liu, H., G. Canton, C. Yuan, C. Yang, K. Billiar, Z. Teng, et al. Using in vivo Cine and 3D multi-contrast MRI to determine human atherosclerotic carotid artery material properties and circumferential shrinkage rate and their impact on stress/strain predictions. J. Biomech. Eng. 134(1):011008, 2012.

39. Marque, V., H. Van Essen, H. A. Struijker-Boudier, J. Atkinson, and I. Lartaud-Idjouadiene. Determination of aortic elastic modulus by pulse wave velocity and wall tracking in a rat model of aortic stiffness. J. Vasc. Res. 38(6):546–550, 2001.

40. Millasseau, S. C., A. D. Stewart, S. J. Patel, S. R. Redwood, and P. J. Chowienczyk. Evaluation of carotid-femoral pulse wave velocity: influence of timing algorithm and heart rate. Hypertension 45(2):222–226, 2005.

41. Peng, H.-H., H.-W. Chung, H.-Y. Yu, and W.-Y. I. Tseng. Estimation of pulse wave velocity in main pulmonary artery with phase contrast MRI: preliminary investigation. J. Magn. Reson. Imaging 24(6):1303–1310, 2006.

42. Rabben, S. I., N. Stergiopulos, L. R. Hellevik, O. A. Smiseth, S. Slørdahl, S. Urheim, et al. An ultrasound-based method for determining pulse wave velocity in superficial arteries. J. Biomech. 37(10):1615–1622, 2004.

43. Ruesink, T., R. Medero, D. Rutkowski, and A. Roldán-Alzate. In vitro validation of 4D flow MRI for local pulse wave velocity estimation. Cardiovasc. Eng. Technol. 9(4):674–687, 2018.

44. Schäfer, M., D. D. Ivy, S. H. Abman, A. J. Barker, L. P. Browne, B. Fonseca, et al. Apparent aortic stiffness in children with pulmonary arterial hypertension: existence of vascular interdependency? Circ. Cardiovasc. Imaging 10(2):e005817, 2017.

45. Schievano, S., A. M. Taylor, C. Capelli, L. Coats, F. Walker, P. Lurz, et al. First-in-man implantation of a novel percutaneous valve: a new approach to medical device development. EuroIntervention 5(6):745–750, 2010.

46. Sugawara, J., T. Tomoto, and H. Tanaka. Heart-to-brachium pulse wave velocity as a measure of proximal aortic stiffness: MRI and longitudinal studies. Am. J. Hypertens. 32(2):146–154, 2019.

47. Swift, A. J., S. Rajaram, R. Condliffe, D. Capener, J. Hurdman, C. Elliot, et al. Pulmonary artery relative area change detects mild elevations in pulmonary vascular resistance and predicts adverse outcome in pulmonary hypertension. Investig. Radiol. 47(10):571–577, 2012.

48. Taylor, C. A., and C. A. Figueroa. Patient-specific modeling of cardiovascular mechanics. Annu. Rev. Biomed. Eng. 11(1):109–134, 2009.

49. Tiwari, K. K., S. Bevilacqua, G. Aquaro, P. Festa, L. Ait-Ali, and M. Solinas. Evaluation of distensibility and stiffness of ascending aortic aneurysm using magnetic resonance imaging. JNMA 55(204):67–71, 2016.

50. Vulliémoz, S., N. Stergiopulos, and R. Meuli. Estimation of local aortic elastic properties with MRI. Magn. Reson. Med. 47(4):649–654, 2002.

51. Wentland, A. L., T. M. Grist, and O. Wieben. Review of MRI-based measurements of pulse wave velocity: a biomarker of arterial stiffness. Cardiovasc. Diagn. Ther. 4(2):193–206, 2014.

52. Westenberg, J. J. M., E. P. van Poelgeest, P. Steendijk, H. B. Grotenhuis, J. W. Jukema, and A. de Roos. Bramwell-Hill modeling for local aortic pulse wave velocity estimation: a validation study with velocity-encoded cardiovascular magnetic resonance and invasive pressure assessment. J. Cardiovasc. Magn. Reson. 9(14):2, 2012.

53. Wittek, A., W. Derwich, K. Karatolios, C. P. Fritzen, S. Vogt, T. Schmitz-Rixen, et al. A finite element updating approach for identification of the anisotropic hyperelastic properties of normal and diseased aortic walls from 4D ultrasound strain imaging. J. Mech. Behav. Biomed. Mater. 58:122–138, 2016.

54. Zambrano, B. A., N. A. McLean, X. Zhao, J.-L. Tan, L. Zhong, C. A. Figueroa, et al. Image-based computational assessment of vascular wall mechanics and hemodynamics in pulmonary arterial hypertension patients. J. Biomech. 8(68):84–92, 2018.

Acknowledgments

This research work was funded by VIVIR Project (Italian Ministry of Health, PE-2013-02357974 Grant) and British Heart Foundation (PG/17/6/32797).

Conflict of interest

None to declare.